Approximation method for fast calculation of transmission in multi-mode waveguides

MARIA PASZKIEWICZ,[1,2,*] **MARIIA SUKHOVA,**[3] **WILLY DÖRFLER,**[3] AND **CARSTEN ROCKSTUHL**[1,4]

[1]*Institute of Theoretical Solid-State Physics (TFP), Karlsruhe Institute of Technology, Karlsruhe, Germany*

[2]*Scientific Computing Center (SCC), Karlsruhe Institute of Technology, Karlsruhe, Germany*

[3]*Institute for Applied and Numerical Mathematics (IANM), Karlsruhe Institute of Technology, Karlsruhe, Germany*

[4]*Institute of Nanotechnology (INT), Karlsruhe Institute of Technology, Karlsruhe, Germany*

*maria.paszkiewicz@kit.edu

Freeform dielectric waveguides connect optical chips made of different materials in fully integrated photonic devices. With a spatial extent in the order of 100 μm, they constitute a computational challenge and make Maxwell full-wave solvers unhandy for the accelerated design. Therefore, it is of utmost importance to have tools that permit the fast prediction of waveguide loss to enable the rapid optimization of waveguide trajectories. Previously developed methods relied on the assumption that only a single mode propagates in the waveguide. However, the propagation of higher-order modes is not just unavoidable due to the geometry of the waveguides, but also, sometimes, beneficial as it increases the number of channels to transmit information. In this contribution, we present an approximate method for the fast calculation of transmission that accommodates the presence of higher-order waveguide modes, and assess its liability by describing light propagation through selected devices.

1. INTRODUCTION

Allowing for the propagation of higher-order modes in waveguides has attracted attention in silicon photonics. The associated increase in the number of channels to transmit data in mode-division-multiplexed systems [1], where multiple guided modes carry signals, is quite appealing. Additionally, multi-mode silicon-on-insulator (SOI) waveguides enable direct coupling between few-mode optical fibers and photonic chips [2,3]. Other applications of silicon waveguides sustaining higher-order modes are for on-chip polarization-handling devices [4] and on-chip add–drop optical filter b ased o n a multi-mode Fabry–Perot cavity [5]. Moreover, and from a general perspective, permitting multi-mode transmission and waveguide shapes deviating from a straight path expands the possibilities of waveguide design. It was shown that the flexibility and compactness of the photonic devices [6,7] is possible if bending is exploited [7–10].

In addition to SOI waveguides, three-dimensional freeform optical waveguides facilitate the transmission of electromagnetic waves between different components of optical chips made from incompatible materials that constitute complex photonic circuits [11]. In particular, III-V semiconductors are highly suitable for all active components, e.g., for light generation and detection [12]. In contrast, Si or SiO_2 based optical chips provide many mature functionalities for passive optical components. These different components can be assembled into a sophisticated architecture by connecting them with freeform optical waveguides, usually called photonic wire bonds. However, when placing the different chip components onto a common substrate within a certain accuracy, in mass production, their exact positions may differ from sample to sample. To account for inaccuracies in the positioning of the chips, the waveguide connections (photonic wire bonds) are fabricated *in situ* by high-resolution 3D laser lithography [13–15]. Such a fabrication approach offers unprecedented control over the waveguide trajectory. After inspecting the spatial locations of input and output ports, an optimal trajectory with the least transmission loss must be calculated. With a target of a fabrication cycle of at most tens of seconds, a fast and reliable strategy is needed to compute the optimal trajectory offering the least loss. This optimization requires a tool to predict the loss accurately and reliably [16]. A full-wave numerical solution to Maxwell's equations is not an option as the spatial extent of the waveguides can be on the order of hundreds of micrometers [17], too large to cope with the time constraints of the optimization.

Therefore, to discuss all these systems mentioned above, simplified methods are urgently needed for the fast modeling of large optical waveguiding structures, for which a numerical solution to Maxwell's equations (utilizing the finite element method or finite-difference time-domain approach) is no longer feasible. One attempt to predict the transmission through

freeform waveguides is based on the *fundamental mode approximation* (FMA) [16]. There, it was assumed that the energy is carried along the waveguide only by a fundamental mode for a given polarization. Then, an arbitrary trajectory of a photonic wire bond can be sliced into segments with a constant radius of curvature. The total loss can be computed by summing up the bending and transition losses. Bending loss occurs in segments of bent waveguides and is linked to the complex-valued propagation constant [18]. In contrast, transition loss occurs at the interface between two waveguide segments with different radii of curvature. In the FMA, they are calculated from the transmission coefficient of the fundamental mode sustained in adjacent waveguide segments. The results of this approach agree with those obtained by numerical simulation for simple-shaped waveguides. However, the FMA does not fully agree with experiments, showing higher loss for advanced trajectories [17]. Moreover, no framework has been developed to acquire information about the transmission of higher-order modes in such an approximate setting. Such ability might be of use in the efficient design of multi-mode waveguides.

To circumvent these issues, we present in Section 2 a solution to this challenge and describe the extension of the FMA to the multi-mode approximation (MMA). The MMA can describe the light propagation in curved waveguides. For the moment, we consider only waveguides where a curvature changes in a single dimension. The presented method intends to overcome the limitations of the FMA when the waveguides support multiple modes [17]. That happens, for example, in spatial regions with a sudden change in the radius of curvature. There, the light is coupled with a notable amplitude to the higher-order modes, which affects the transmission of the fundamental mode. Similarly to the FMA, the MMA relies on the precomputation of modal properties of guided modes for a set of radii of curvature, which we describe in Sections 2.A and 2.B. While the precomputation of modal properties is not necessary for the actual method, it accelerates the prediction of loss tremendously, a prerequisite for prospective optimization. Sections 2.C and 2.D describe in detail the propagation and transition loss in the case of the MMA, respectively. The method is summarized in Section 2.E. In Section 3, the MMA is used on an example of a waveguide comprising two interfaces between straight and bend segments and a waveguide composed of arcs of alternating curvature sign. The results are benchmarked with numerical simulations performed with CST Microwave studio [19]. The improvement to the previously considered FMA is clearly demonstrated, paving the way for the future efficient exploration of photonic wire bonds.

2. MULTI-MODE APPROXIMATION

The basic approach of the MMA consists in tracking the amplitudes of a few selected modes that are guided along the waveguide with an, in general, arbitrary smooth trajectory. The curves should be C^2, with at least a C^1 connection between the straight and curved parts [20]. The waveguide with the arbitrary trajectory is sliced into a finite number of segments within which the radius of curvature is constant. Then, we can describe the propagation in each waveguide segment as a multiplication of the modal amplitudes with an exponential

function. The exponential function contains in its argument the length of the waveguide segment multiplied by the complex propagation constant of the respective mode. Here, the mode accumulates a certain phase, and its amplitude lowers because of nonvanishing radiation loss. At the interface between the waveguide segments with different radii of curvature, a transmission matrix is calculated to express the inter- and intra-mode transmission coefficients. Here, the orthogonality is broken, and the modes can mutually couple. Calculating the entries of these transmission matrices requires us to know the tangential field profiles of the modes. To speed up later simulations, the modal properties are precomputed for a finely sampled radius of curvature. A quantity that we call the *t*-maps expresses the transmission coefficients between waveguide segments of different radii of curvature. Without loss of generality, we consider the case in which two modes are supported in the waveguide, and the trajectories are confined to a single plane.

For a comprehensive discussion, we start this section by initially outlining how to compute a bent waveguide's guided modes and outline aspects concerning their orthogonality. Afterward, we track the amplitudes of the modes upon propagation and at the transition between segments with different radii of curvature. The latter is condensed in the *t*-maps. Finally, we outline how to stitch all these aspects together and calculate the total transmission through a multi-mode waveguide with an arbitrary trajectory.

A. Solution on Cross Section

The photonic wire bonds considered in this work have a rectangular cross section. Such waveguides confine light in two transverse directions (x and y), and the modes are guided along the waveguide core for which the effective refractive index n_{eff} satisfies the condition $n_{clad} \leq n_{eff} \leq n_{core}$ [21–23]. For waveguides studied here, with the parameters [17] height 1.8 μm, width 2.0 μm, wavelength 1.55 μm, refractive index of the core $n_{core} = 1.53$ and the cladding $n_{clad} = 1.36$, the mode analysis shows propagation of six modes. In fact, there are three quasi-transverse-electric (TE) modes, and the same number of quasi-transverse-magnetic (TM) modes is supported [24]. Such a waveguide geometry motivates us to consider a multi-modal approach to predict the transmission with such an approximation method.

The electric and magnetic fields of propagating modes in a waveguide cross section perpendicular to the direction of propagation are computed with the commercially available finite element method (FEM) solver JCMsuite [25] by solving Maxwell's equations in source-free media in the frequency domain [26–28]. The field distribution and propagation constants are obtained by solving Maxwell's equations as an eigenvalue problem [29]. Although only two-dimensional cross sections are considered, the software accommodates a possible bending and twisting of the waveguide.

JCMsuite allows us to determine several modes propagating in the waveguide. Field profiles differ in amplitude, shape, and orientation (and number) of positive and negative extrema. The real part of the x component of the normalized electric field of three selected mode profiles is exemplarily shown in Fig. 1 for a straight (upper row) and bent waveguide (bottom
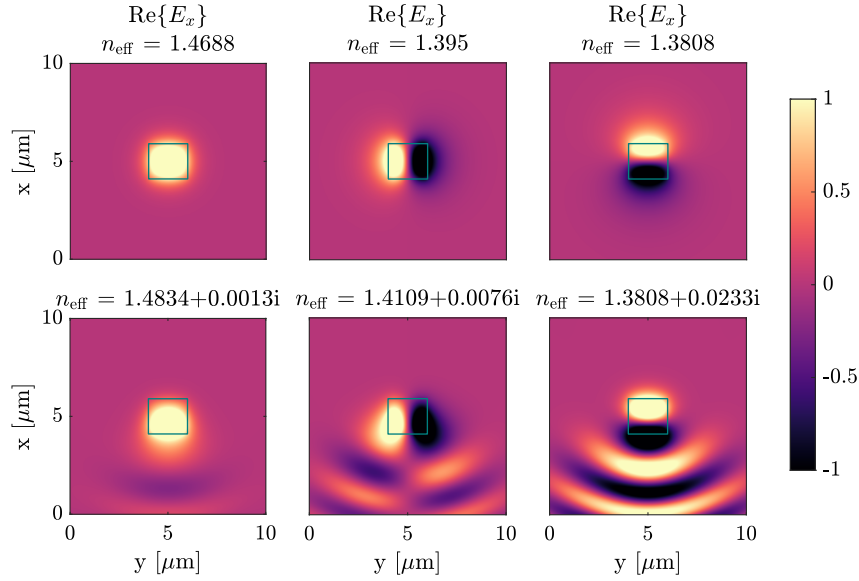
Fig. 1. Mode profiles of the real part of the x component of the normalized electric field obtained with JCMsuite for a straight (top) and bend waveguide (bottom) of radius of curvature 20 μm, bent along the x axis. All fields are normalized to the maximum amplitude of the fundamental mode of the straight waveguide. Three lowest-order modes of the same polarization are considered here, and the figures contain information on the effective refractive index. Each mode is normalized to the maximum amplitude of the strongest mode (characterized by $n_{\text{eff}} = 1.4688$). The core of the waveguide is marked with a green rectangle. It is surrounded by the cladding. The computational domain has been limited to a 10 μm × 10 μm square.

row). The modes are sorted according to their descending effective refractive index $n_{\text{eff}} = k_0^{-1}\beta$, with vacuum wavelength k_0 and propagation constant β. In this work, we consider two propagating modes. Besides the fundamental mode with a given polarization, we will consider as the second higher-order mode the mode with the same polarization and a symmetry that permits a coupling in the presence of a finite curvature. For a curvature in the x direction, the mode shall have the same symmetry in the y direction and one more amplitude node into the x direction, as can be seen in the third column in Fig. 1.

In the presence of a finite curvature, the mirror symmetry of the modes regarding the x or y axis is broken (depending on the considered direction of the curvature). That happens because the modes tend to localize in the outer region of the waveguide and are no longer centered in the core. In Fig. 1, we clearly see that with a smaller radius of curvature, the center of gravity of the mode shifts away from the center of the waveguide.

Moreover, the onset of a finite radiation loss causes these fields to oscillate outside the waveguide. This broken mirror symmetry then allows coupling between modes at interfaces of waveguide segments with different radii of curvature, as the mode profiles start to overlap. Such coupling influences the transmission between adjacent waveguide segments, something we aim to capture in the MMA. Figure 1 shows that the fields of the fundamental and the third-order propagating modes are characterized by preserved symmetry in the y direction for two different radii of curvature.

The effective refractive index differs for different modes. Figure 2 shows how the real [Fig. 2(a)] and imaginary parts [Fig. 2(b)] of the effective refractive index change depending on the considered mode and the radius of curvature of the waveguide. Note that we consider here a curvature in the x direction. The real part of n_{eff} expresses the phase accumulation of the modes upon propagation, and the imaginary part is a measure
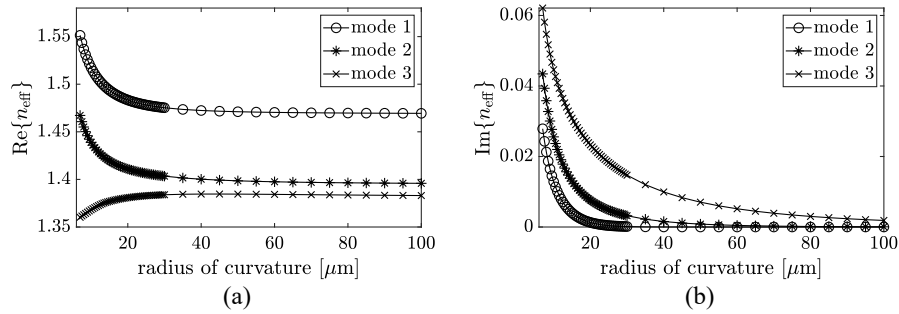
Fig. 2. Dependence of (a) real part and (b) imaginary part of effective refractive index on the radius of curvature of the waveguide for the three lowest-order modes. The radius of curvature in this work is measured from the center of curvature to the center of the waveguide. The effective refractive index of the respective mode m is related to the propagation constant β_m by $n_{\text{eff}}^m = k_0^{-1}\beta_m$.

of the modal amplitude attenuation. We clearly see that with decreasing radius of curvature, the imaginary part of the refractive index increases, reminiscent of the onset of the bending loss. The modes are no longer guided but are weakly coupled to the continuum of free-space modes.

B. Orthogonality of Guided Modes

The propagating light in the waveguide can be expressed as a superposition of its eigenmodes. Each guided waveguide mode is characterized by transverse field amplitude profiles. Following the ket notation from [30,31], the mode is expressed as

$$|\mathbf{M}_j^{\pm}\rangle = \left(e_{j,x}, e_{j,y}, \pm h_{j,x}, \pm h_{j,y}\right)^{\mathrm{T}}, \tag{1}$$

where $e_{j,x}$, $e_{j,y}$, $h_{j,x}$, and $h_{j,y}$ denote, respectively, x and y components of electric and magnetic field profile of the jth mode, and the $\pm$ superscript refers to the forward or backward propagation direction, along the z axis.

The electric and magnetic fields are normalized to obtain unit power flow in the propagation direction for the lossless propagating modes [16], according to

$$\langle \mathbf{M}_i | \mathbf{M}_j \rangle = \frac{1}{4} \int_S \left(\mathbf{e}_i \times \mathbf{h}_j + \mathbf{e}_j \times \mathbf{h}_i\right) \cdot \hat{\mathbf{z}}\, dx\, dy = \begin{cases} 1, & i = j \\ 0, & i \neq j \end{cases}. \tag{2}$$

The above expression comes from the time-averaged energy flux given by the real part of the complex Poynting vector. For both absorbing and nonabsorbing waveguides holds the unconjugated form of the orthogonality relation [32]. The integration is performed over the infinite cross section S, perpendicular to the propagation direction $\hat{\mathbf{z}}$. It can be interpreted as projection of the ith mode $|\mathbf{M}_i\rangle$ onto the jth mode $|\mathbf{M}_j\rangle$.

The integral in Eq. (2) is defined over the infinite space. Since this cannot be accommodated in practice, it requires choosing a finite computational domain. As a consequence, the values of the integral (2) oscillate in an exponentially damped manner as a function of domain size and converge to the proper value as the size reaches infinity. To obtain the limit t_0, we first compute the value of (2) (and, indeed, all similar expressions that will follow) for different computational domain sizes ℓ that we summarize in a function $\ell \mapsto f(\ell)$. Then, the functional dependency of the computed data is fitted to the expression

$$f(\ell) = t_0 + \mathrm{Re}\left\{2 \cdot A \exp(B\ell)\right\}, \tag{3}$$

with A and B being complex parameters. Optimal values of all parameters are found iteratively with Matlab's *fminsearch* function [33]. From a practical perspective, it turned out that it is enough to limit the computational domain to 10 μm × 10 μm in the case of straight waveguide and bends of low curvature. To increase the accuracy for bending, where the mode leaks to the cladding, the domain was extended in the outer bow direction, into which the mode stretches, to 20 μm.

The modes are computed for a discrete set of radii of curvature. The radii span to consider here is large—starting from 7 μm up to infinity, corresponding to a straight waveguide. The lower bound for the radius results from our approach that is geared towards waveguide trajectories with low loss. There, the coupling between the modes and their attenuation is merely a

perturbation. Such an assumption only holds for reasonably large radii of curvature. For excessively small radii of curvature, the modes are no longer guided, and the loss is tremendous. Waveguides with such sharp bends are usually not considered in practical PWBs. However, there are works [8–10,34] on bends of 10 μm and below, which are already considered as very sharp. To determine a finite set of radii, it is important to determine the upper bound of the radius for which the waveguide can be assumed to be straight. Here, the radius 1000 μm was chosen. This value is justified by the tiny rate of change of the fields for radii starting from 100 μm (i.e., 10% of the limit value). Also, the computation time increases vastly for higher radii of curvature. When precomputing the modes, the values of radii do not need to be spaced equally. The variation of the fields is higher for smaller bending radii, and, therefore, a higher sampling rate applies to radii smaller than 50 μm. The sampling is coarser with a weaker bending. The modes guided by the bent waveguide are computed for each radius of curvature from the set. Once the modes are calculated for waveguides of different radii or curvature, the loss can be analyzed in detail. We do so in the following subsections.

C. Bending: Propagation Loss

A waveguide is called *lossy* if the amount of energy carried by the electromagnetic field at the waveguide's output is smaller than the input energy. Loss does not occur in a straight waveguide with an invariant cross section made of a nonabsorbing material. Any deviation from these ideal conditions causes loss [17]. Therefore, the loss occurs if the waveguide is no longer straight (*bending loss*) but also if its geometry changes, e.g., the radius of curvature or the cross section size (*transition loss*) [20,35]. These are the loss mechanisms that are considered in this work. Further loss can be caused by the quality of fabrication or material impurities [16]. However, their significance is usually minor, so they are not considered here.

The bending loss is quantified by the imaginary part of the propagation constant of the mode [36]; see Fig. 2(b). The transmission of the mode m along the bent segment n scales with

$$\exp\left((\mathrm{iRe}\,\{\beta_m(R_n)\} - \mathrm{Im}\,\{\beta_m(R_n)\})\, l\right),$$

where l is the length of the segment and R_n denotes its radius of curvature. Note the sign convention in the exponent, suggesting a positive value of the imaginary part of the propagation constant.

D. Interface Problem: Transition Loss

Once we have determined the loss experienced by each mode upon propagation through a curved segment of the waveguide, we need to compute the change in their amplitudes at the intersection between two waveguide segments with different radii of curvature.

For that purpose, we consider the transmission through the plane that separates two waveguide segments of different curvatures. In that scenario, one encounters an *interface problem* sketched in Fig. 3.
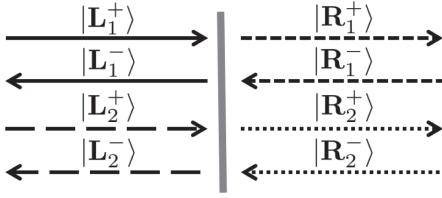
Fig. 3. Two forward propagating incident modes $|\mathbf{L}_1^+\rangle$ and $|\mathbf{L}_2^+\rangle$ on the left-hand side of the interface that are transmitted into two forward propagating modes $|\mathbf{R}_1^+\rangle$ and $|\mathbf{R}_2^+\rangle$ on the right-hand side of the interface. The incident modes are also reflected at the interface and propagate back as modes $|\mathbf{L}_1^-\rangle$ and $|\mathbf{L}_2^-\rangle$. On the right-hand side, there are also backward propagating modes $|\mathbf{R}_1^-\rangle$ and $|\mathbf{R}_2^-\rangle$ present. They are created by reflection from consecutive interfaces or could also be present if the principal propagation direction had been reversed.

There, an arbitrary superposition of modes $|\mathbf{L}_n^+\rangle$ impinging on the interface causes excitation of modes $|\mathbf{L}_n^-\rangle$ and $|\mathbf{R}_n^+\rangle$ in reflection and transmission, respectively. The impinging modes can also be scattered into a continuum of radiation modes, $|\mathbf{L}_q^-\rangle$ or $|\mathbf{R}_q^+\rangle$. At the output side, the backward propagating modes $|\mathbf{R}_n^-\rangle$, reflected from the next interface, are present. However, they are not included in the computation as their influence on the transmission is minor. For that, the necessary multiple reflections do not yield a sizable amplitude. Due to the continuity of the tangential field components on the interface between the two segments, the sum of the modal fields on the inlet (left) must be equal to the sum of the modes at the outlet (right) [30,37]:

$$\sum_n i_n \, |\mathbf{L}_n^+\rangle + \sum_n r_n \, |\mathbf{L}_n^-\rangle + \int r_q^- \, |\mathbf{L}_q^-\rangle \, \mathrm{d}q$$

$$= \sum_n t_n \, |\mathbf{R}_n^+\rangle + \int r_q^+ \, |\mathbf{R}_q^+\rangle \, \mathrm{d}q, \tag{4}$$

where r_n and t_n denote the reflection and transmission coefficients, respectively, and i_n marks the amplitude distribution among the incident modes. The difference between profiles of the fundamental modes $|\mathbf{L}_1^+\rangle$ and $|\mathbf{R}_1^+\rangle$ results in the excitation of higher-order and radiation modes at the interface. This effect is quantified by the values of the inner product (2) between the modes propagating in adjacent waveguide segments. It is not necessary to consider all the achievable modes in the expansion, but only those modes that propagate to the following waveguide segments without too much loss and that are excited at the interface in a representative situation by a notable amplitude. In the following, it will be assumed that the waveguide is excited with the fundamental mode. However, at the positions where the radius of curvature changes, higher-order modes are excited as they are necessary to satisfy the interface condition with a better accuracy than in the FMA, as expressed in Eq. (4).

To solve the relation (4) for the scattering coefficients r_n and t_n, we project the $\langle\mathbf{R}_n^+|$ and $\langle\mathbf{R}_n^-|$ on both sides, in the case of each mode. The number of considered modes N leads then to the set of $2N$ equations. Consideration of two modes results in the following set of equations:

$$i_1\langle\mathbf{R}_1^+|\mathbf{L}_1^+\rangle + i_2\langle\mathbf{R}_1^+|\mathbf{L}_2^+\rangle + r_1\langle\mathbf{R}_1^+|\mathbf{L}_1^-\rangle + r_2\langle\mathbf{R}_1^+|\mathbf{L}_2^-\rangle$$

$$= t_1\langle\mathbf{R}_1^+|\mathbf{R}_1^+\rangle + t_2\langle\mathbf{R}_1^+|\mathbf{R}_2^+\rangle, \tag{5}$$

$$i_1\langle\mathbf{R}_2^+|\mathbf{L}_1^+\rangle + i_2\langle\mathbf{R}_2^+|\mathbf{L}_2^+\rangle + r_1\langle\mathbf{R}_2^+|\mathbf{L}_1^-\rangle + r_2\langle\mathbf{R}_2^+|\mathbf{L}_2^-\rangle$$

$$= t_1\langle\mathbf{R}_2^+|\mathbf{R}_1^+\rangle + t_2\langle\mathbf{R}_2^+|\mathbf{R}_2^+\rangle, \tag{6}$$

$$i_1\langle\mathbf{R}_1^-|\mathbf{L}_1^+\rangle + i_2\langle\mathbf{R}_1^-|\mathbf{L}_2^+\rangle + r_1\langle\mathbf{R}_1^-|\mathbf{L}_1^-\rangle + r_2\langle\mathbf{R}_1^-|\mathbf{L}_2^-\rangle$$

$$= t_1\langle\mathbf{R}_1^-|\mathbf{R}_1^+\rangle + t_2\langle\mathbf{R}_1^-|\mathbf{R}_2^+\rangle, \tag{7}$$

$$i_1\langle\mathbf{R}_2^-|\mathbf{L}_1^+\rangle + i_2\langle\mathbf{R}_2^-|\mathbf{L}_2^+\rangle + r_1\langle\mathbf{R}_2^-|\mathbf{L}_1^-\rangle + r_2\langle\mathbf{R}_2^-|\mathbf{L}_2^-\rangle$$

$$= t_1\langle\mathbf{R}_2^-|\mathbf{R}_1^+\rangle + t_2\langle\mathbf{R}_2^-|\mathbf{R}_2^+\rangle. \tag{8}$$

Some terms disappear due to the orthogonality relations (2). Rearranging the above equations allows us to write the formulas for transmission and reflection coefficients in a concise matrix form:

$$\mathbf{t} = \begin{pmatrix} \langle\mathbf{R}_1^+|\mathbf{R}_1^+\rangle & \langle\mathbf{R}_1^+|\mathbf{R}_2^+\rangle \\ \langle\mathbf{R}_2^+|\mathbf{R}_1^+\rangle & \langle\mathbf{R}_2^+|\mathbf{R}_2^+\rangle \end{pmatrix}^{-1} \begin{pmatrix} \langle\mathbf{R}_1^+|\mathbf{L}_1^+\rangle & \langle\mathbf{R}_1^+|\mathbf{L}_2^+\rangle \\ \langle\mathbf{R}_2^+|\mathbf{L}_1^+\rangle & \langle\mathbf{R}_2^+|\mathbf{L}_2^+\rangle \end{pmatrix}$$

$$= \begin{pmatrix} t_{11} & t_{12} \\ t_{21} & t_{22} \end{pmatrix} \begin{pmatrix} i_1 \\ i_2 \end{pmatrix} = \hat{\boldsymbol{t}}\mathbf{i}, \tag{9}$$

$$\mathbf{r} = -\begin{pmatrix} \langle\mathbf{R}_1^-|\mathbf{L}_1^-\rangle & \langle\mathbf{R}_1^-|\mathbf{L}_2^-\rangle \\ \langle\mathbf{R}_2^-|\mathbf{L}_1^-\rangle & \langle\mathbf{R}_2^-|\mathbf{L}_2^-\rangle \end{pmatrix}^{-1} \begin{pmatrix} \langle\mathbf{R}_1^-|\mathbf{L}_1^+\rangle & \langle\mathbf{R}_1^-|\mathbf{L}_2^+\rangle \\ \langle\mathbf{R}_2^-|\mathbf{L}_1^+\rangle & \langle\mathbf{R}_2^-|\mathbf{L}_2^+\rangle \end{pmatrix} = \hat{\boldsymbol{r}}\mathbf{i}, \tag{10}$$

where $\mathbf{r} = (r_1, r_2)^{\mathrm{T}}$ and $\mathbf{t} = (t_1, t_2)^{\mathrm{T}}$ are the vectors of reflection and transmission coefficients, respectively. Note that the formula for the reflection coefficient is shown for completeness and will not be used in the following approximation method. The vector $\mathbf{i} = (i_1, i_2)^{\mathrm{T}}$ denotes the incident field distribution. In the case of an incident single-mode field impinging onto the interface, its amplitude is expressed as the fundamental mode, denoted as $\mathbf{i} = (1, 0)^{\mathrm{T}}$. In the transmission matrix $\hat{\boldsymbol{t}}$, each entry expresses the transmission from a waveguide segment left to the interface to a waveguide segment right to the interface. The coefficients t_{11} and t_{22} are, therefore, interpreted as a measure of modes 1 and 2 transmitted through the interface as modes 1 and 2, respectively. At the same time, coefficient t_{12} (t_{21}) means the fraction of mode 2 (1) coupled to mode 1 (2). The fundamental mode and one higher-order mode, resulting in the highest values of off-diagonal coefficients t_{12} and t_{21}, are considered in the presented MMA.

The dimensions of the matrices appearing in Eqs. (9) and (10) depend on the number of modes considered. In this work, they are 2×2 matrices, while in the case of one mode only, the coefficients are the same as in the case of the FMA.

E. *t*-maps

To account for transitions between segments of arbitrary radii of curvature, a lookup table of transmission coefficients, later called *t-maps*, is generated. The computation is performed for each combination of radii from the set in Section 2.B. To refine the values of transmission coefficient, the Matlab function *griddata* was used to interpolate the known values of transmission to the finer set of radii of curvature. The t-maps were created separately for real (Fig. 4) and imaginary parts (Fig. 5) of all the entries of the transmission matrix.
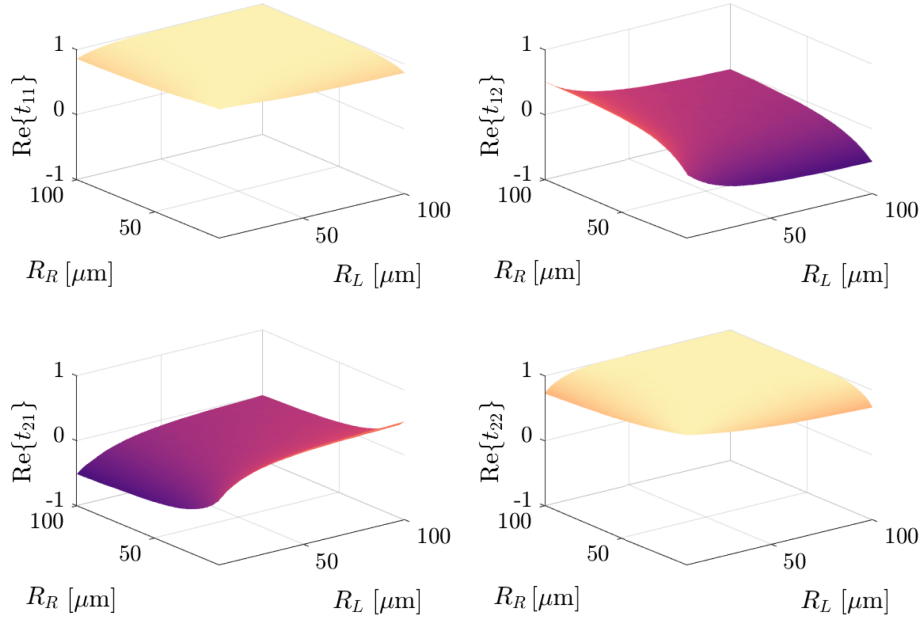
Fig. 4. Separate maps for the real part of each entry of the transmission matrix $\hat{t}$. The coefficients are calculated for every combination of bending radii of adjacent segments from the chosen set. For readability, the shown range is cut at 100 μm.
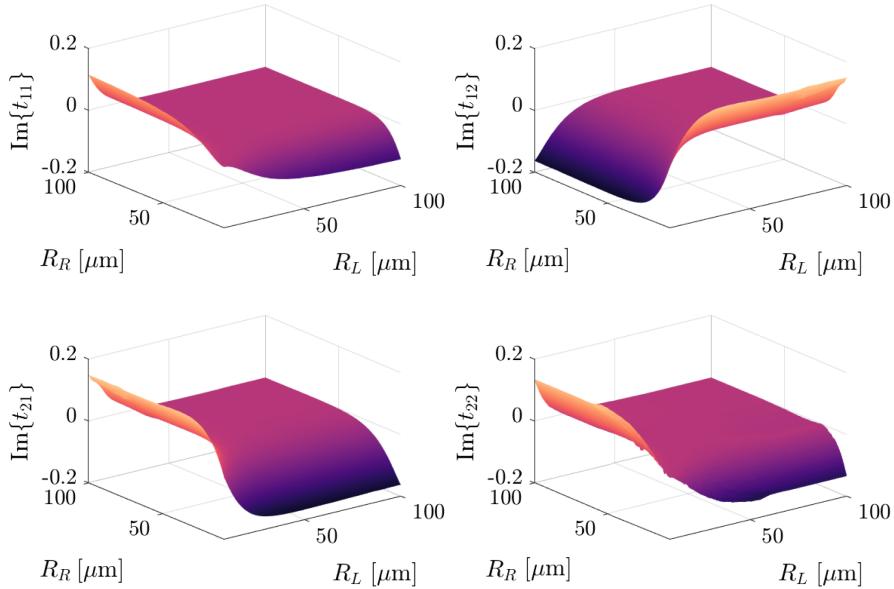

Fig. 5. Separate maps for the imaginary part of each entry of the transmission matrix $\hat{t}$. The coefficients are calculated for every combination of bending radii of adjacent segments from the chosen set. For readability, the shown range is cut at 100 μm.

The t-map presented here does not account for a change in sign of curvature after passing an inflection point. Nevertheless, in optimization procedures the purpose is to find waveguide trajectories with low loss, so a smooth transition between segments is expected. Basic intuition suggests that this requires rather a gradual change of the waveguide curvature where no sudden variation of the bending radius happens, especially not a change in sign. This intuition is corroborated by selected full-wave simulations using CST Microwave Studio of the light propagation through a sequence of segments in which the radius of curvature is constant. Specifically, we consider four waveguide segments: straight–bend–bend–straight. Here, the sign of the radius of

curvature of the two bent segments is once the same [Fig. 6(a)] and once different [Fig. 6(b)]. The absolute values of electric field amplitudes in a central cross section of the waveguide (in the x-z-plane at $y = 0$) are shown. We also indicate the total transmission into the fundamental mode in both configurations. It can be seen that while both configurations suffer from the same bending loss and the same loss at the interface between the straight and the bend segments, the total transmission in the case of the S-bend is much smaller than in the case of the C-bend. The abrupt change in sign in the radius of curvature in the case of the S-bend simply causes that additional loss. Hence, an abrupt sign change should be avoided. Figure 6(c) shows

(a) C-bend (b) S-bend (c) S-bend, adiabatic
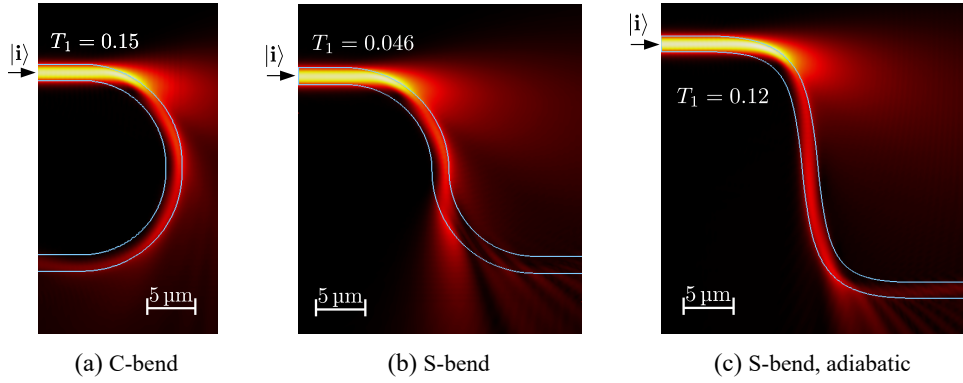
Fig. 6. Absolute value of the amplitude of the electric field upon considering the fundamental mode of a straight waveguide as the illumination in case of a waveguide composed of two arcs of (a) same sign and radius 10 μm, (b) same radius of curvature 10 μm but with opposite sign, and (c) S-bend of comparable size but gradual change of curvature with the smallest bending radius 6 μm.
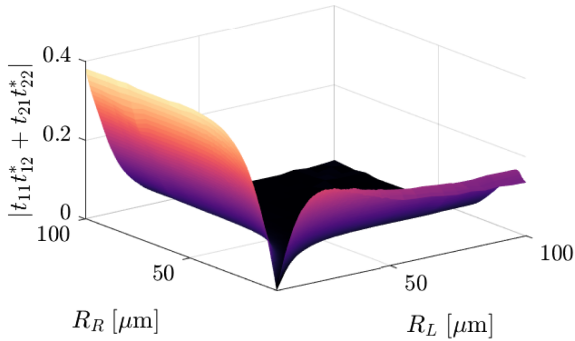
Fig. 7. Assessment of the energy loss at the interface between two waveguide segments. The values deviating from zero express the loss of energy at the interface to modes not considered in the respective subset of modes whose amplitudes are tracked in the MMA. The onset of such energy loss may limit the applicability of the MMA, restricted to two propagating modes, for certain combinations of bending radii, especially when the segments of low curvature are connected to sharply curved segments.

additionally an *S*-bend of the same cross section and comparable size, where the curvature was modeled as a sine function multiplied with the reciprocal of the radius of curvature, with a minimum radius of curvature 6 μm. This allows a continuous change of the radius of curvature and avoids abrupt changes. Although the minimum bending radius is smaller than in the case of the simple *S*-bend, the transmission is close to the model with constant sign of radius of curvature thanks to the smooth transition of the radius of curvature.

To judge the losses of a given transition between two waveguide segments, we analyze conservation relations between incoming and outgoing optical powers. The entries of the transmission matrix should satisfy the condition $t_{11}t_{12}^* + t_{21}t_{22}^* = 0$ in the case of a lossless system [21]. The absolute value of the left-hand side of this condition is presented in Fig. 7. Nonzero values for the high *curvature contrast* suggest higher energy loss and so increasing inaccuracy of the approximation method.

F. Segmentation of the Trajectory

Having computed the t-maps and propagation constants, the power loss in a waveguide of arbitrary trajectory in a 2D plane can be calculated. Although a fully 3D problem is considered, the possible bend of a waveguide is allowed only in one direction.

Because the orientation of the waveguide in 3D does not influence the transmission, the waveguide path can be described as a series of arcs of given radius of curvature and arc length. The radii smaller than the lower bound of 7 μm are set as equal to it, and those above the upper limit of 1000 μm are treated as straight segments.

The waveguide trajectory is divided into $N + 1$ segments, from which the first and last one are assumed to be straight and serve the propagation of input mode $|\text{in}\rangle$ and output mode $|\text{out}\rangle$. The segments are connected by N interfaces marked with double vertical lines in Fig. 8.

The illumination of a waveguide with an input signal in the fundamental mode is expressed as an amplitude vector denoted by $|\text{in}\rangle = (1, 0)^{\text{T}}$. The incoming field encounters the interface $\boxed{1}$, where the amplitude distribution is modified by multiplication with the complex $\hat{t}_1$ matrix corresponding to the transmission through the first interface. The fields continue propagating through the segment, in which they can attenuate and accumulate phase due to bending. Each mode propagates according to different complex propagation constant, which can be indicated by multiplication with a propagation matrix

$$\hat{p}_n = \begin{pmatrix} \exp\left((i\text{Re}\{\beta_1(R_n)\} - \text{Im}\{\beta_1(R_n)\})\,l\right) & 0 \\ 0 & \exp\left((i\text{Re}\{\beta_2(R_n)\} - \text{Im}\{\beta_2(R_n)\})\,l\right) \end{pmatrix} \quad \textbf{(11)}$$

with $n = 1$, which contains the values of propagation constant both for fundamental, subscript 1, and second higher-order mode, subscript 2, propagating in the waveguide segment of length l and radius of curvature R_n.
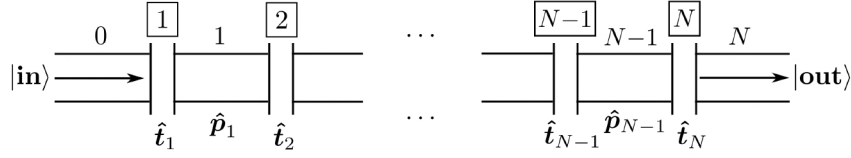
Fig. 8. Separation of a waveguide trajectory into segments of constant radius of curvature labeled with integer numbers from 0 to N. The first and the last segments are straight. The interfaces are numbered from 1 to N.

The multiplication is repeated for the subsequent interfaces and segments between them. Eventually, the amplitude transmission through the entire freeform waveguide can be calculated as

$$\mathbf{T} = \hat{\boldsymbol{t}}_N \hat{\boldsymbol{p}}_{N-1} \hat{\boldsymbol{t}}_{N-1} \cdots \hat{\boldsymbol{t}}_2 \hat{\boldsymbol{p}}_1 \hat{\boldsymbol{t}}_1 |\mathbf{in}\rangle. \qquad (12)$$

Due to the matrix multiplication, it is important to indicate input and output of the waveguide, because the result may differ for the opposite propagation direction. The transmission of particular mode amplitudes can then be read from $\mathbf{T} = (T_1, \ T_2)^{\mathrm{T}}$. The value of T_1^2 corresponds to the power transmission of the fundamental mode at the waveguide output, while T_2^2 describes the power fraction carried by the second higher-order mode. These are the quantities of interest that we wish to discuss for a waveguide of a given trajectory.

3. RESULTS

We apply our approximate method in the following to three carefully chosen examples: a 90° bow, a waveguide composed of alternating arcs, and an S-bend with a continuous curvature change. The results obtained with the MMA are compared to the FMA and full-wave solutions. We rely on CST Microwave Studio for that purpose. CST Microwave Studio simulations are performed using the time-domain solver based on the finite integration technique (FIT) [19]. The mesh density, defined by the number of discretization cells per wavelength, was set to 10. Local mesh refinements at the core boundaries and curved surfaces are done automatically to increase the accuracy. The computational domain is a cuboid enclosing the entire waveguide. To compute and visualize the field amplitude distribution properly, a space is left between the waveguide core and the walls of the computational domain. The boundaries of the computational domain are set to open, which is equivalent to the PML method [19,38]. At one end of the waveguide, an input port 1 and, at the opposite end, an output port 2 are defined, which is important for S-matrix computations [39,40]. The S-matrix contains the fractions of complex amplitudes scattered through port 1 or 2 upon exciting the system through either port 1 or 2. The S-matrix relates each mode of each waveguide port with the rest of the modes. The off-diagonal matrix components represent transmission (or reflection) from one mode of a waveguide port into another mode of another waveguide port. In contrast, diagonal components represent the reflection of each mode back into the same mode.

All numerical simulations in CST Microwave Studio and the calculation of the modal amplitudes when using the MMA and FMA, for which computation times are compared, were performed on a desktop computer with processor Intel Core i7-7700 CPU @ 3.60 GHz, min. 16 GB RAM. All waveguide simulations were performed with the same CST acceleration settings: CPU acceleration up to two devices and four CPU threads. The time-consuming precomputation of modes and t-maps was performed on an external computer cluster.

A. 90° Bow

A 90° bow is the simplest shape of practical interest [7,9,10], which contains two interfaces where the modes can couple: straight-bend and bend-straight. It is a classical example, where intramode mismatch and intermode coupling occurs, resulting in loss and intermode cross-talk [1]. The bend section in the following is assumed to take 90°. Figure 9 (left) shows, at the example of a curved waveguide with a radius of curvature of 10 μm, that the majority of loss occurs at the first interface. Of course, this is only meant in an absolute sense. At the interface between the waveguide segments with different radii of curvature, a notable fraction of the field is coupled to free-space radiation and emerges as a loss. In Fig. 9 (right), we compare the transmission computed with FMA, MMA, and full-wave simulation. The transmissions are derived here from the amplitudes in the final straight waveguide segment. The figure shows good agreement between transmission of both fundamental and higher-order modes between full-wave simulations and the approximate methods. A slight difference between MMA and FMA can be observed for very sharp bends, below 15 μm. For this range of radii of curvature, the solutions diverge slightly from the reference computed with CST due to high transmission loss. Similarly, the differences occur in the case of high damping of the second mode for a waveguide bend approaching a straight segment. The slight drop in the transmission of the second-order mode near the radius of curvature 20 μm is compensated by the increment in transmission of the next mode (not shown in the Fig. 9 due to low transmission). The limitation of MMA to two modes justifies its insensibility to this effect.

The functional dependency of the transmission coefficients is also quite intuitive. For a very large radius of curvature, the smooth variation of the modal properties causes a negligible mismatch between the modes supported in the different segments, and the transmission is nearly perfect into the fundamental mode. The next higher-order mode is negligibly excited. For a decreasing radius of curvature, the next higher-order mode gets increasingly excited, and the lowest-order mode shows a reduced transmission. For extreme radii of curvature, the transmission drops all together in both modes because of the onset of coupling to radiating modes at the interfaces. In Fig. 9 (right) the CST results for the transmission of the second mode are fluctuating because the discretization accuracy in the simulation is reached. However, the overall decreasing tendency is noticeable.
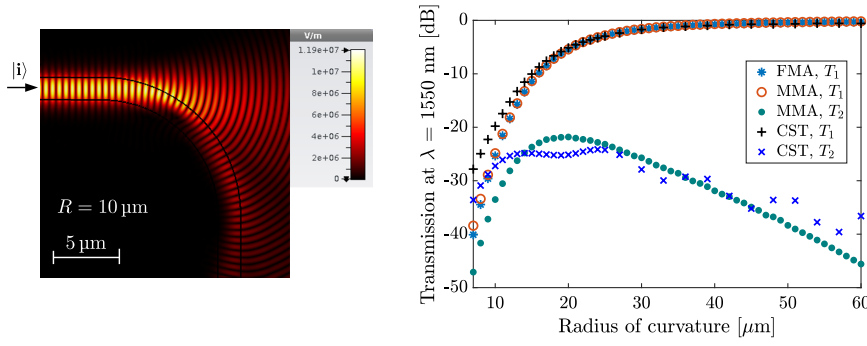
Fig. 9. Magnitude of the instantaneous electric field in a dielectric waveguide of a straight–bend–straight form upon considering the fundamental mode of a straight waveguide as the illumination (left). Comparison of corresponding power transmitted in fundamental mode T_1 and second higher-order mode T_2 as a function of radius of curvature (right).

However, from our perspective, the most important aspect is the accelerated prediction of the transmission in these scenarios. The time to compute the results with the MMA with 94 trajectories, sliced into 1-μm-long segments, ranging from bending radius 7 μm to 100 μm, was approximately 24 s. In contrast, the full-wave simulations of 32 bends, ranging from 6 μm to 60 μm, using CST, took 7 h and 20 min. Of course, the precomputation of the modal properties and the t-maps cannot be neglected. That took approximately four days (without parallelization) for 88 radii of curvature. These 2D simulations considering the waveguide cross sections gave the full information needed to proceed with MMA.
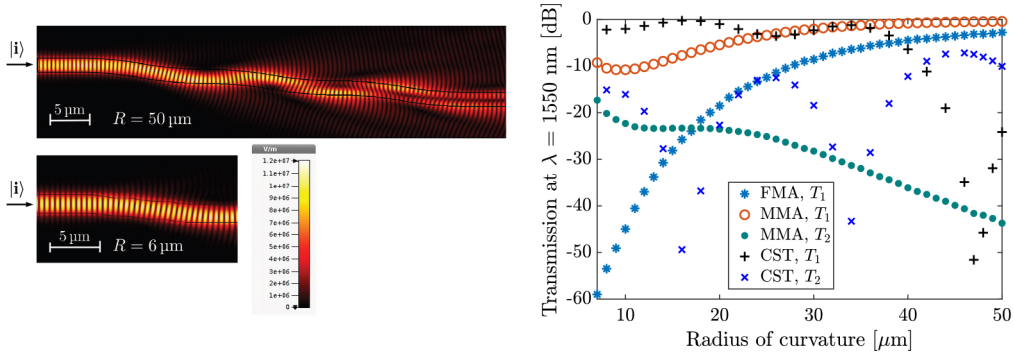
B. Snake-Shaped Waveguides

Another example is waveguides created from a series of six arcs of an angle 10° and the same absolute value of radius of curvature but alternating sign. Because of this shape, they are called here *snake*-shaped waveguides. This form is particularly interesting because of periodicity and so the significance of the propagation constants of the modes. The example is an extreme case that allows us to capture some of the limiting aspects of the MMA.

Figure 10 (right) compares the transmission computed with the three methods for radii of curvature ranging from 7 μm to 50 μm. The figure clearly shows that the FMA is not sufficient to predict the transmission correctly. The transmission of the fundamental mode computed with the MMA approaches the

reference and coincides with it for a range of curvatures. The transmission is mostly determined by the radius of curvature, so it generally increases with increasing bending radius. At the same time, the reference simulations show two aspects of importance. First, the transmission drops tremendously above a radius of curvature of roughly 40 μm for the 10° arc segments. The periodicity imposed by the periodic change of the radius of curvature causes a drastic change in the response, presumably due to mode coupling and scattering loss. The transmission into the fundamental mode is entirely suppressed for a critical radius of curvature. This is partially illustrated in the left of Fig. 10, where the electric field in the cross section of the waveguide trajectory is shown. Also, since the MMA (and the FMA anyhow) do not consider the presence of backward propagating modes, they could not capture related effects and could not correctly predict the transmission. However, while the MMA can capture the details outside that resonant regime, it continues to provide not so accurate predictions for extremely small radii of curvature. This resembles the limitations seen already in the previous example.

Transmission for 45 trajectories was calculated in 6 s with MMA, while the time of full-wave simulations in CST varied from 5.5 min to 21.5 min for the smallest to biggest bending radius displayed in the plot in Fig. 10.

Fig. 10. Magnitude of the instantaneous electric field in a dielectric waveguide of a *snake*-shaped form, with different radii of curvature, upon considering the fundamental mode of a straight waveguide as the illumination (left). Transmission of the fundamental and second-order mode calculated with use of different methods (right).
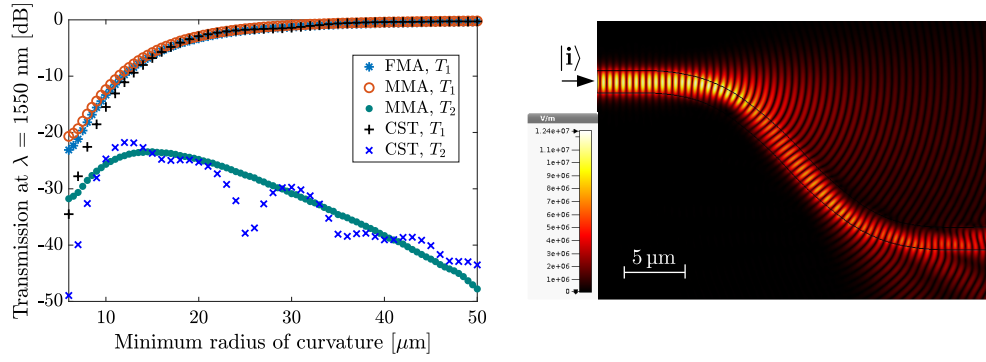
Fig. 11. Transmission of fundamental and second-order mode as a function of the minimum bending radius for an S-bend with continuous change of curvature (left). Magnitude of the instantaneous electric field in a dielectric waveguide of a S-shaped form, with a minimum radius of curvature 10 µm, upon considering the fundamental mode of a straight waveguide as the illumination (right).

C. *S*-Bend with Adiabatic Change of Curvature

The last example considered here is an S-bend, in which the curvature was modeled as $\kappa = (r_{min})^{-1} \sin \varphi$, where r_{min} is the minimum radius of curvature of a waveguide and the angle φ ranges from 0 to 2π. The results are presented in Fig. 11. Although there is a change of curvature sign, the curvature changes smoothly (up to the discretization of angle φ) so the approximation methods should be applicable; see Fig. 6. Transmission of the fundamental mode is slightly more accurate with MMA than FMA. Predicted transmission of the second-order mode is much higher than the reference in the case of a very small minimum radius of curvature. The reference results suggest that the remaining transmitted power is distributed to a similar extent among the higher modes.

The time to compute the results with the MMA for 89 trajectories was approximately 53 s. In contrast, the full-wave simulations using CST took from 11 min 14 s for the shortest trajectory up to 4 h 52 min 9 s in case of the longest trajectory considered for Fig. 11.

4. CONCLUSIONS

In the core of this work, we described an approximation method to calculate the transmission of a fundamental and a next higher-order mode in a curved waveguide trajectory. We showed its application on three exemplary shapes of 3D waveguides. In this method, the trajectory is approximated with discrete arcs. The total loss is composed of accumulated propagation loss in the segments and transmission between the adjacent arcs. The method takes into consideration the possible coupling between two propagating modes, which is quantified by the transmission matrix. Multiplication of the propagation and transmission matrices results in the total transmission. Comparison of the approximated results to the reference transmission, computed with the full-wave solver CST Microwave Studio, shows that the approximation methods are reliable for transmission of the fundamental mode in trajectories with continuous change of curvature. MMA is applicable also for trajectories composed of a few segments only. FMA remains a fast and robust method to calculate transmission in single-mode 3D waveguides and so can be applied as a merit function to optimize their trajectory. In the cases where the change of curvature excites higher-order modes,

MMA makes it possible to quickly calculate the transmission of higher-order modes and so the MMA gives more accurate results for transmission. It reduces computation time significantly from hours to tenths of seconds. MMA is more sensitive to the accuracy of the calculated transmission coefficients, as compared to FMA. Therefore, it may in this form not be applicable to complex trajectories, made of sharp bends with bending radius lower than 20 µm.

Disclosures. The authors declare no conflict of interest.

Data availability. Data underlying the results presented in this paper are not publicly available at this time but may be obtained from the corresponding author upon reasonable request.

REFERENCES

1. C. Li, D. Liu, and D. Dai, "Multimode silicon photonics," Nanophotonics **8**, 227–247 (2018).
2. Y. Lai, Y. Yu, S. Fu, *et al.*, "Compact double-part grating coupler for higher-order mode coupling," Opt. Lett. **43**, 3172–3175 (2018).
3. D. Dai and M. Mao, "Mode converter based on an inverse taper for multimode silicon nanophotonic integrated circuits," Opt. Express **23**, 28376–28388 (2015).
4. D. Dai and J. E. Bowers, "Novel concept for ultracompact polarization splitter-rotator based on silicon nanowires," Opt. Express **19**, 10940–10949 (2011).
5. Q. Huang, Q. Liu, and J. Xia, "Traveling wave-like Fabry–Perot resonator-based add-drop filters," Opt. Lett. **42**, 5158–5161 (2017).
6. D. Dai, "Advanced passive silicon photonic devices with asymmetric waveguide structures," Proc. IEEE **106**, 2117–2143 (2018).
7. C. Sun, Y. Yu, G. Chen, *et al.*, "Ultra-compact bent multimode silicon waveguide with ultralow inter-mode crosstalk," Opt. Lett. **42**, 3004–3007 (2017).
8. H. Wu, C. Li, L. Song, *et al.*, "Ultra-sharp multimode waveguide bends with subwavelength gratings," Laser Photon. Rev. **13**, 1800119 (2019).
9. Y. Liu, W. Sun, H. Xie, *et al.*, "Very sharp adiabatic bends based on an inverse design," Opt. Lett. **43**, 2482–2485 (2018).
10. M. Teng, A. A. Noman, Y. J. Lee, *et al.*, "A 3-micron-radius bend for SOI TE0/TE1 multiplexing," in *Conference on Lasers and Electro-Optics* (Optica, 2018), paper JW2A.13.
11. M. Blaicher, M. R. Billah, J. Kemal, *et al.*, "Hybrid multi-chip assembly of optical communication engines by in situ 3D nano-lithography," Light Sci. Appl. **9**, 71 (2020).

12. D. Thomson, A. Zilkie, J. E. Bowers, *et al.*, "Roadmap on silicon photonics," J. Opt. **18**, 073003 (2016).

13. N. Lindenmann, G. Balthasar, D. Hillerkuss, *et al.*, "Photonic wire bonding: a novel concept for chip-scale interconnects," Opt. Express **20**, 17667–17677 (2012).

14. M. R. Billah, M. Blaicher, T. Hoose, *et al.*, "Hybrid integration of silicon photonics circuits and InP lasers by photonic wire bonding," Optica **5**, 876–883 (2018).

15. N. Lindenmann, "Photonic wire bonding as a novel technology for photonic chip interfaces," Ph.D. thesis (Karlsruhe Institute of Technology, 2017).

16. F. Negredo, M. Blaicher, A. Nesic, *et al.*, "Fast and reliable method to estimate losses of single-mode waveguides with an arbitrary 2D trajectory," J. Opt. Soc. Am. A **35**, 1063–1073 (2018).

17. A. Nesic, M. Blaicher, E. Orlandini, *et al.*, "Transformation-optics modeling of 3D-printed freeform waveguides," Opt. Express **30**, 38856–38879 (2022).

18. K. R. Hiremath, M. Hammer, R. Stoffer, *et al.*, "Analytic approach to dielectric optical bent slab waveguides," Opt. Quantum Electron. **37**, 37–61 (2005).

19. Dassault Systèmes, "CST studio suite CST microwave studio," 2018, https://www.3ds.com/products-services/simulia/products/cst-studio-suite/solvers/.

20. R. Baets and P. E. Lagasse, "Loss calculation and design of arbitrarily curved integrated-optic waveguides," J. Opt. Soc. Am. **73**, 177–182 (1983).

21. B. E. Saleh and M. C. Teich, *Fundamentals of Photonics* (Wiley, 2019).

22. X. Wang, C. Yin, and Z. Cao, "Transfer matrix method and the graded-index waveguide," in *Progress in Planar Optical Waveguides* (Springer, 2016), pp. 17–42.

23. S. Nanz, "Tailored light scattering and emission in solar cells and LEDs using ordered and disordered interfaces," Ph.D. thesis (Karlsruhe Institute of Technology, 2019).

24. K. Okamoto, *Fundamentals of Optical Waveguides*, 2nd ed. (Elsevier, Acadamic, 2006).

25. JCMwave GmbH Berlin, "JCMsuite documentation," 2019, https://www.jcmwave.com/docs/ParameterReference/2abc74e9a16d20eacf2c6a0991083041.html?version=5.4.1.

26. J. D. Jackson, *Classical Electrodynamics*, 3rd ed. (Wiley, 1999).

27. A. V. Lavrinenko, J. Lægsgaard, N. Gregersen, *et al.*, *Numerical Methods in Photonics* (CRC Press, 2018).

28. J.-M. Jin, *The Finite Element Method in Electromagnetics*, 3rd ed. (Wiley-IEEE, 2014).

29. J. R. Cardoso, *Electromagnetics Through the Finite Element Method: A Simplified Approach Using Maxwell's Equations* (CRC Press, 2016).

30. T. Paul, "Light propagation in optical metamaterials: a Bloch modal approach," Ph.D. thesis (Friedrich-Schiller-Universität Jena, 2012).

31. T. Paul, C. Menzel, W. Śmigaj, *et al.*, "Reflection and transmission of light at periodic layered metamaterial films," Phys. Rev. B **84**, 115142 (2011).

32. A. W. Snyder and J. D. Love, *Optical Waveguide Theory* (Champman and Hall, 1983).

33. The MathWorks Inc., MATLAB version: 9.5.0.944444 (R2018b) (2018).

34. L. Ebers, M. Hammer, and J. Förstner, "Oblique incidence of semi-guided planar waves on slab waveguide steps: effects of rounded edges," Opt. Express **26**, 18621–18632 (2018).

35. M. Hammer, L. Ebers, and J. Förstner, "Oblique quasi-lossless excitation of a thin silicon slab waveguide: a guided-wave variant of an anti-reflection coating," J. Opt. Soc. Am. B **36**, 2395–2401 (2019).

36. K. Hiremath, R. Stoffer, and M. Hammer, "Modeling of circular integrated optical microresonators by 2-D frequency domain coupled mode theory," Opt. Commun. **257**, 277–297 (2006).

37. W. Śmigaj, P. Lalanne, J. Yang, *et al.*, "Closed-form expression for the scattering coefficients at an interface between two periodic media," Appl. Phys. Lett. **98**, 111107 (2011).

38. P. Bienstman, E. Six, A. Roelens, *et al.*, "Calculation of bending losses in dielectric waveguides using eigenmode expansion and perfectly matched layers," IEEE Photon. Technol. Lett. **14**, 164–166 (2002).

39. G. Lecamp, J. P. Hugonin, and P. Lalanne, "Theoretical and computational concepts for periodic optical waveguides," Opt. Express **15**, 11042–11060 (2007).

40. A. Krasnok, D. Baranov, H. Li, *et al.*, "Anomalies in light scattering," Adv. Opt. Photon. **11**, 892–951 (2019).